Effect of Air Gap Thickness on Transverse-Flux Permanent Magnet (TFPM) Machines with Flux-Concentration

M. R. Dubois,
Eocycle Technologies Inc
49, Bel-Air, Suite 106
Lévis, Québec, Canada
phone: (418) 833-8144
e-mail: mdubois@eocycle.com,

H.Polinder and J.A. Ferreira
Laboratory of Electrical Power Processing
Delft University of Technology
Mekelweg 4, 2628 CD Delft, The Netherlands,
+31 15 278 6259 – fax: +31 15 278 29 68 –
h.polinder@its.tudelft.nl, j.a.ferreira@its.tudelft.nl,

***Abstract* — The use of Transverse-Flux Permanent Magnet (TFPM) machines for high-torque and low-speed application is investigated. The ability of TFPM structures with flux-concentration to reduce the cost of active material is looked upon more closely. The Cost/Torque characteristics of TFPM (Transverse-Flux Permanent Magnet) machines and Conventional Permanent Magnet Synchronous machines are presented. It is emphasized how the air gap thickness plays a dominant role in the cost savings provided by the TFPM structure. For air gap of 0.5 mm, the TFPM structure with flux concentration discussed in the paper shows important cost benefits, over the Conventional Permanent Magnet Synchronous machine. Above the 3.5 mm threshold, the TFPM with flux concentration does not show such great cost advantages over the Conventional Permanent Magnet Synchronous machine.**

1. Introduction

Many applications require electrical machines with high torque and low speed. Such applications are: wind turbine generators, ship propulsion motors, bus traction motors. The use of a gearbox with a low-torque machine is often preferred to the direct-drive machine with high torque, mainly because of the high costs of direct-drive electrical machines.

To reduce the cost of the direct-drive machines, the use of Transverse-Flux Permanent Magnet (TFPM) structures is investigated. TFPM machines make possible the use of short pole pitches in combination with high current loading. In most TFPM machine prototypes built, this gives a torque over mass ratio higher than conventional machines. A reduction in the active mass will also lead to a reduction in the cost of active material. The costs for active material for the TFPM machine with flux-concentration and for the Conventional Permanent Magnet Synchronous machines (PMSM) are compared. Both machine types are modeled and optimization programs are developed, which target the lowest cost/torque for generator diameters between 0.5 m to 4 m. Attention is paid to the effect of airgap thickness on the cost/torque ratios of both machine types.

2. Machine structures investigated

Among the several topologies of the TFPM concept, the TFPM machine with double-sided air gap and flux-concentration is chosen for this investigation. This structure was proposed in [1], and is shown in fig. 1. As discussed in [2], TFPM structures with flux-concentration make a better use of the PM material, and have higher air gap flux density than TFPM machines with surface magnets.

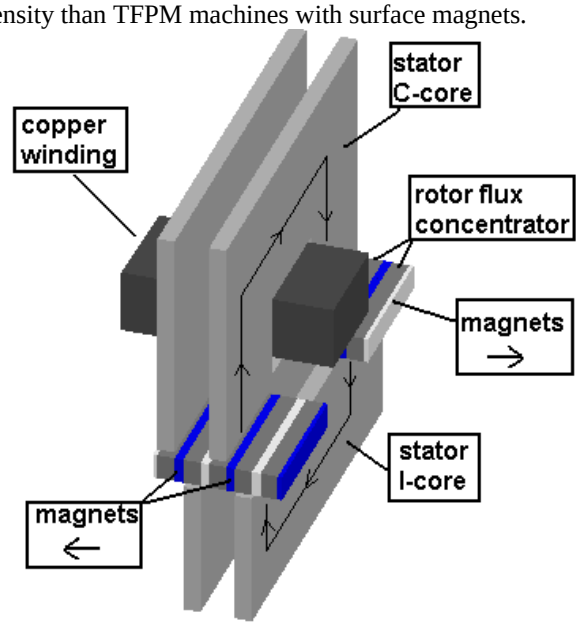

Fig.1. TFPM machine with flux-concentration. Linear representation.

This TFPM structure is chosen, because it was the first TFPM structure with flux-concentration proposed in the literature, and from which most other TFPM structures with flux-concentration (as in [3]) are derived. The conclusions of this paper will apply to most of TFPM machines with flux-concentration.

The second machine structure analyzed in the paper is the Conventional PMSM, shown in fig. 2.

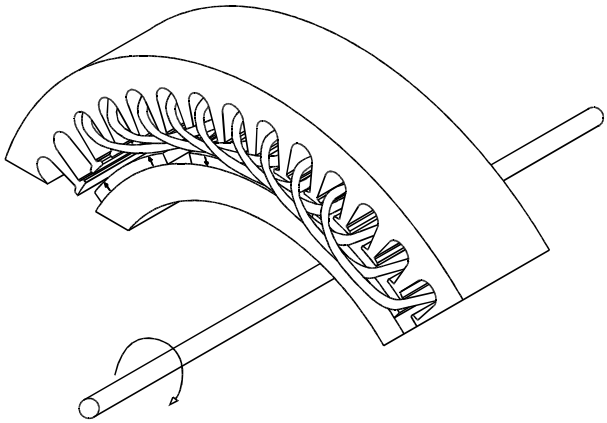

Fig. 2. Conventional PM Synchronous machine.

A. Cost over Torque ratio

The criterion "cost over torque" is used in order to compare the two PM machine geometries. For each of the two machine types, the cost of active material is computed by weighting each material with a given specific cost:

- specific cost of laminated steel = 6 Euro/kg
- specific cost of copper = 6 Euro/kg
- specific cost of PM = 40 Euro/kg
- specific cost of powdered iron = 6 Euro/kg

3. Performance of TFPM and Conventional PMSM with increasing air gaps

Appendix I describes the analytical models used for torque computation. Using the machine models developed in Appendix I, two optimization programs were developed, which vary all geometrical parameters, and calculate the corresponding torque and corresponding cost. The programs retain the lowest value of the cost over torque ratio. For the TFPM machine, the torque of the optimal design is checked by implementing the cost-optimal geometry in a 3-D finite element analysis (FEA) software.

Optimal designs of the Conventional PMSM and TFPM machine are calculated for diameters varying between 0.5 m and 4 m, and for air gap thickness varying between 0.5 mm and 4 mm. The resulting cost over torque ratios are presented in fig. 3 and fig. 4.

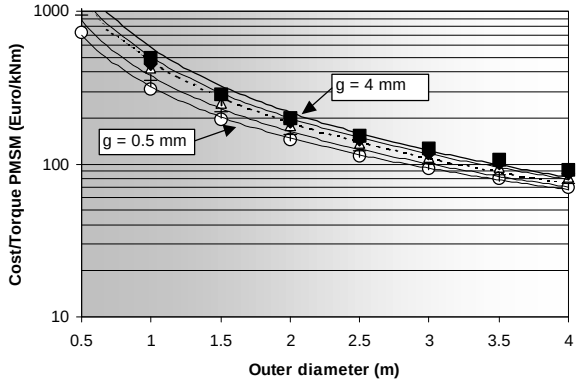

Fig. 3. Cost / Torque of optimized Conventional PMSM. Air gap thickness (in mm): 0.5, 1, 2, 3, 4.

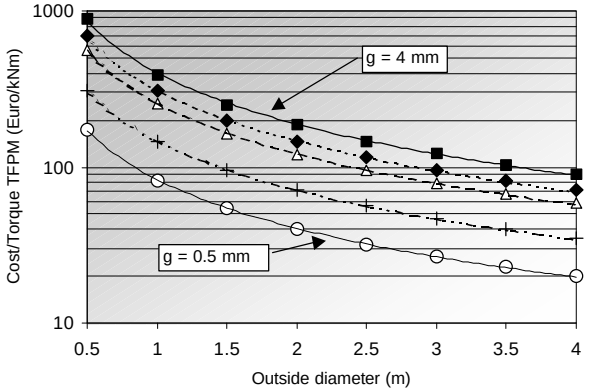

Fig. 4. Cost / Torque of optimized TFPM. Air gap thickness (in mm): 0.5, 1, 2, 3, 4.

Inspection of fig. 3 indicates only little influence of the air gap thickness on the cost over torque ratio, in the case of the Conventional PMSM. For the TFPM machine, the cost over torque ratio (fig. 4) is much more sensitive to air gap thickness variations. It must be noted that the optimization process targeted machine designs with similar efficiencies (fixed to 92% in this case). The efficiency has a significant influence on the cost over torque ratio, which is not covered in the paper.

Fig. 5 shows the TFPM cost advantage factor K_{TFPM_Cost}, as defined by (1).

$$K_{TFPM\_Cost} = \frac{Cost/Torque\_PMSM}{Cost/Torque\_TFPM} \qquad (1)$$

Fig. 5 shows that the TFPM machine with flux-concentration provides a significant cost advantage over the Conventional PMSM for an air gap of 0.5 mm. However, this advantage is reduced when the air gap increases. The TFPM machine with flux-concentration is a good choice for cost reduction in active material. However, the air gap thickness should be maintained below 3 mm, in order to provide a good cost advantage. Fig. 3 and 4 also indicated that increasing the diameter also reduces the cost of active material. An interesting combination for cost reduction would be to use a TFPM machine with flux-concentration, with a large diameter and a thin air gap.

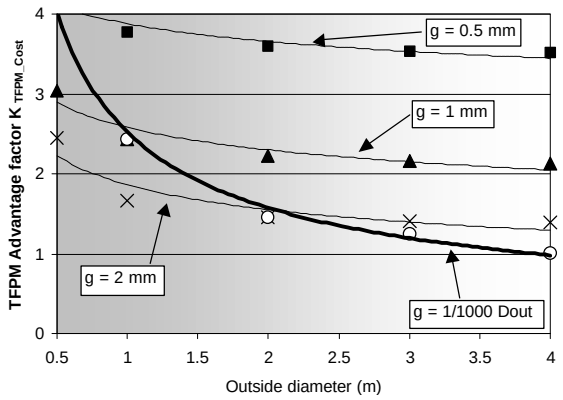

Fig. 5. Cost advantage factor of the TFPM machine over the Conventional PMSM. Square = air gap 0. 5 mm, Triangle = 1 mm, Cross = 2 mm, Circle = 1/1000 of outside diameter.

However, mechanical considerations may prevent such a combination to be feasible. If the common practice of using an air gap of $1/1000^{th}$ of the machine outer diameter is used, then the two machine types give comparable cost over torque ratios when used with a 4-meter diameter (see fig. 5). Above that point, we observe that TFPM machines with flux-concentration are no longer an interesting choice.

4. Causes of TFPM sensitivity to air gap thickness

The strength of the TFPM machine is the high degree of

freedom on the pole pitch value. To make the no-load voltage as high as possible, a short pole pitch is normally selected. The drawback of short pole pitches is the presence of strong leakage paths between adjacent flux concentrators. The increase in air gap thickness will increase the air gap reluctance R_g, without changing the reluctances R_{LEC} and R_{ctc} of the leakage paths. These leakage paths are modeled as lumped reluctances in fig. 6.

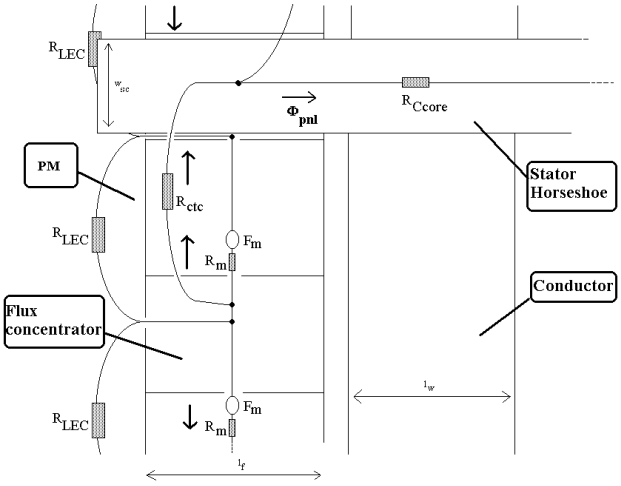

Fig. 6. Top view of the TFPM machine with flux concentration and double-sided air gap, shown in the aligned position. Only one side of the rotor is shown, with the different flux paths replaced by lumped reluctances.

The no-load flux density Φ_{pnl} in the stator core is reduced when the air gap increases. In such cases, equal levels of no-load flux density can be maintained only by:

- increasing the magnet thickness h_m
- increasing the magnet width w_m

In both cases, more flux will travel through the flux concentrators, making saturation a limiting factor. Consequently, the width of the flux concentrator must be increased, resulting in a larger pole pitch. Fig. 7 shows the pole pitch obtained from the optimization programs for the TFPM machine as a function of the air gap thickness.

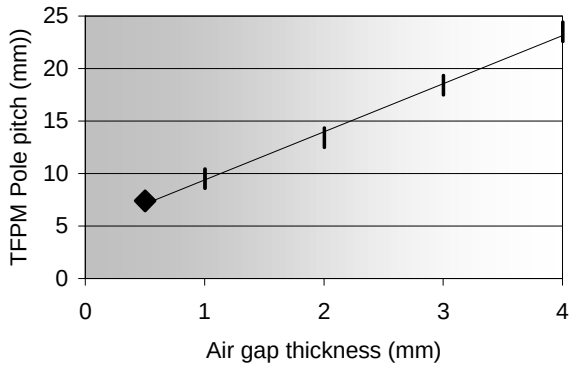

Fig. 7. Pole pitch of the TFPM machine with flux concentration as a function of air gap thickness. The pole pitch is chosen for a design with the minimum cost over torque ratio. The flux concentrators are made of powdered iron, and have a saturation flux density of 1.6 T.

While a 1-mm air gap favors TFPM designs with pole pitches around 10 mm, a 4-mm air gap will favor TFPM designs with pole pitches around 25 mm. According to (9), a same torque is obtained, if the decrease in the number of poles is compensated by an increase in the maximum stator mmf, and an increase in the no-load flux density Φ_{pnl}. The increase in maximum stator mmf also increases the winding window area, the mass of copper winding and the size of the stator cores. Thus, the thicker the air gap thickness, the higher the mass of PM material, copper and iron required for a given torque.

5. Conclusion

The cost over torque ratios of TFPM machines with flux concentration and Conventional PMSM have been investigated. Analytical models have been developed for both machine types. Optimization programs have been developed, allowing the prediction of designs with the lowest cost over torque ratio.

The results of the optimization process are obtained for machine diameters between 0.5 m and 4 m and for air gap thickness of 0.5 mm and 4 mm. The cost over torque ratio of the Conventional PMSM shows a low dependency from the air gap thickness, while the TFPM machine with flux concentration is much more dependent. The TFPM machine with flux concentration shows a cost advantage factor of about 3.5 with an air gap thickness of 0.5 mm. The cost advantage factor decreases to about 1 as the air gap thickness increases to 4 mm. Direct-drive applications can benefit from a TFPM machine with a large diameters and a thin air gap. But in that case, further attention should be given to the mechanical design of such machines.

Acknowledgement

The authors want to thank Delft University Research Institute DU-WIND (The Netherlands) and the Fond pour les Chercheurs et Aide a la Recherche FCAR (Québec, Canada) for financially supporting Mr. Dubois's research.

References

[1] H. Weh, "Permanentmagneterregte Synchronmaschinen hoher Kraftdichte nach dem Transversalflusskonzept," *etzArchiv*, vol. 10, pp. 143-149, 1988.

[2] G. H. Pajooman, Performance Assessment and Design Optimisation of VRPM (Transverse Flux) Machines by Finite Element Computation, Ph.D. dissertation, Dept. Elect. Eng., Univ. Southampton (1997), England.

[3] Maddison C.P., Mecrow B.C. and Jack A.G., "Claw Pole Geometries for High Performance Transverse Flux Machines", in *Proc. ICEM1998*, Vol. 1, pp. 340-345.

[4] A. Grauers, Design of Direct-driven Permanent-magnet Generators for Wind Turbines, Ph.D. dissertation, School Elect. and Computer Eng., Chalmers Univ. Tech. (1996), Göteborg, Sweden.

Appendix I: Mathematical models

The Conventional PMSM and TFPM machine are compared on the basis of their cost over torque ratio.

The two machine types have a large number of geometrical parameters, which can be varied independently, giving out millions of different design possibilities for a same torque rating. To identify the design with the lowest cost over torque ratio, a computer program has been developed for the two machine types. The programs predict the machine torque and cost for each set of geometrical parameters, and allow these geometrical parameters to vary within a certain range.

A. Conventional PMSM: analytical model

The optimization program predicts the torque performance for the Conventional PMSM from its geometrical parameters. The machine torque *T* is derived from (2).

$$T = \frac{P_{mech}}{\Omega} \cong \frac{mEI\cos d}{\Omega} \tag{2}$$

where the no-load losses are neglected, and where the no-load voltage and phase current are assumed as sinusoidal. *E* is derived by using (3), (4) and (5) where (4) was obtained from a 2-D finite element calculation in [4].

$$E = \frac{4}{\sqrt{2}} p k_{ws} B_1 r_g l_s f N_{slot} \tag{3}$$

$$B_1 = \sqrt{2} B_g \left[0.81 - 0.3 \frac{(h_m + g)}{t_p} \right] \tag{4}$$

$$B_g = \frac{\Phi_g}{l_s t_p k_{mag}} \tag{5}$$

Equation (4) is valid for k_{mag} = 0.7. This value has been used in all calculations.

In (3), the stator is assumed as skewed, and k_{ws} is set to 0.95 in the program. The value of Φ_g is obtained by assuming the magnetic field as traveling in straight lines through the magnetic circuit of fig. 8.

In the calculation of R_{stat_teeth}, R_{stat_yoke}, R_{rot_back} , a constant permeability m_{rFe} was used and consequently the machine has been assumed to work below saturation.

The nominal phase current *I* is calculated with (6) and (7).

$$I = JA_{Cus} \tag{6}$$

$$A_{Cus} = k_{sfill} \left[\frac{b_s (h_s - h_w)}{N_{slot}} \right] \tag{7}$$

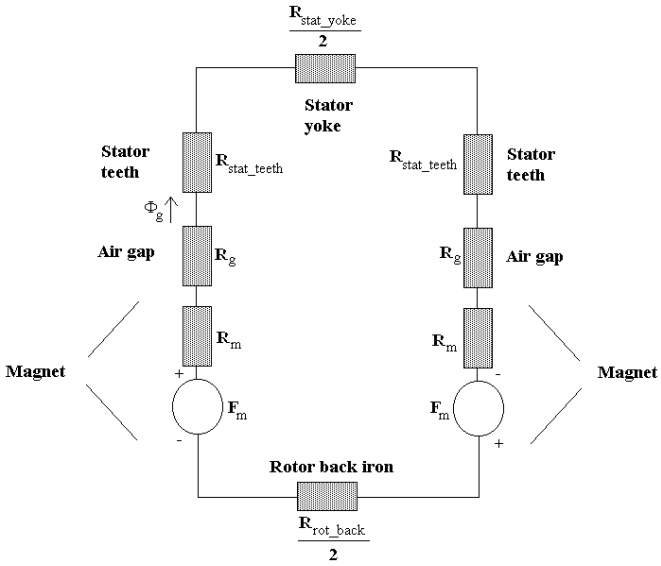

Fig. 8. Magnetic circuit used to determine Φ_g.

In the calculations, the following values are used:

- J = 4.0 A/mm^2
- k_{sfill} = 0.5
- m = 3
- h_w = 5 mm
- slot depth/slot width (h_s/b_s) = 4
- slot width/tooth width = 1.05
- B_r = 1.23 T
- μ_{rFe} = 1000
- μ_{rm} = 1.09
- B_{FEsat} = 1.9 T
- δ = 0 degree
- q = 1
- N_{slot} = 2

B. TFPM machine: analytical model

The TFPM machine is essentially a single-phase machine. It is possible to turn it into a three-phase machine, by stacking three TFPM machines, and shifting their rotors by 120°. The torque of a single-phase machine with salient poles can be expressed as:

$$T \cong \frac{EI}{\Omega}\cos d + \frac{pI^2 f (L_u - L_a)}{2\Omega}\sin 2d \tag{8}$$

where the no-load losses are neglected and where the no-load voltage and phase current are assumed as sinusoidal. The stator inductance is assumed as varying sinusoidally with the electrical angle, between two values L_a and L_u.

Expression (8) is written as a function of the global electrical quantities *E*, *I*, *L*, *f*, Ω. We can also derive a similar expression for *T*, expressed on a per pole-pair basis:

$$T = \frac{p^2}{2} F_s \left[\Phi_{pnl} \cos d + \frac{F_s}{4} \left(\frac{1}{R_{up}} - \frac{1}{R_{ap}} \right) \sin 2d \right] \tag{9}$$

Calculation of F_{pnl} and R_{ap}

In TFPM machines, the pole pitch is generally short. This makes the flux calculation difficult, due to the different leakage paths directed in all 3 dimensions. The leakage flux paths and main paths are shown in fig. 6. The magnetic circuit of fig. 9 represents the combinations of leakage and main paths in the aligned position, modeled by lumped reluctances.

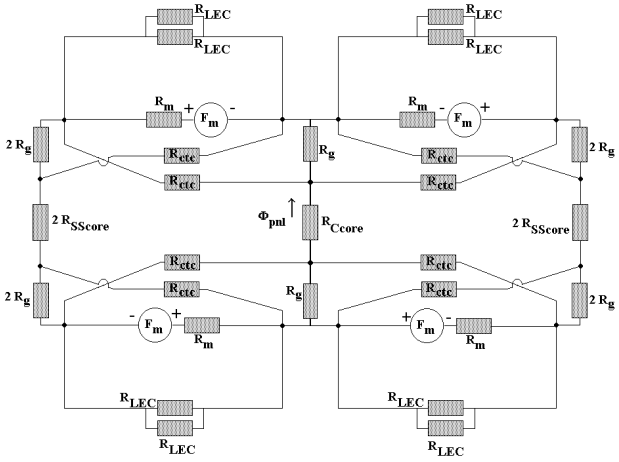

Fig. 9. Magnetic circuit used to determine Φ_{pnl} *and* R_{ap}

The values of Φ_{pnl} and R_{ap} are obtained by solving the magnetic circuit of fig. 9, which gives:

$$\Phi_{pnl} = \frac{F_m(R_{ctc} - 2R_g)}{R_m R_g + 2R_{ctc}\left(2\frac{R_g R_m}{R_{LEC}} + R_g + \frac{R_m}{4}\right) + (R_{Ccore} + R_{SScore})\left(\frac{2R_m R_g + R_m R_{ctc}}{R_{LEC}} + R_g + R_m + \frac{R_{ctc}}{2}\right)} \tag{10}$$

and

$$R_{ap} = R_{Ccore} + R_{SScore} + R_{T12} + \frac{(R_{T2} + R_{ctc})(R_{T1} + 2R_g)}{R_{T1} + R_{T2} + R_{ctc} + 2R_g} \tag{11}$$

where

$$R_{T1} = \frac{R_{ctc} R_m R_{LEC}}{(R_{ctc} + 2R_g)(2R_m + R_{LEC}) + R_m R_{LEC}} \tag{12}$$

$$R_{T2} = \frac{2R_g R_m R_{LEC}}{(R_{ctc} + 2R_g)(2R_m + R_{LEC}) + R_m R_{LEC}} \tag{13}$$

$$R_{T12} = \frac{2R_{ctc} R_g}{R_{ctc} + 2R_g + \frac{R_m R_{LEC}}{2R_m + R_{LEC}}} \tag{14}$$

Calculation of R_{up}

The magnetic circuit in the unaligned position is somewhat simpler. Fig. 10 shows the leakage path for the flux created by the stator winding in the unaligned position.

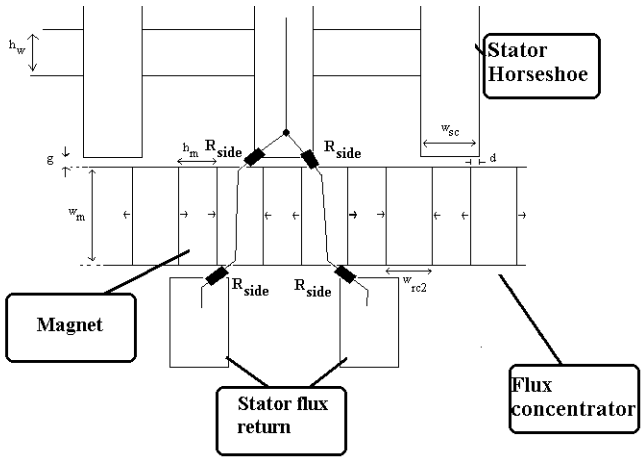

Fig. 10. Side view of the TFPM machine with flux concentration and double-sided air gap, shown in the unaligned position. Only one side of the rotor is shown.

The reluctance R_{up} is then equal to:

$$R_{up} = 2R_{side} \tag{15}$$

Calculation of lumped reluctances

To calculate the value of the lumped reluctances R_m, R_{Ccore}, R_{SScore}, R_{LEC}, R_{ctc}, R_g, R_{side}, and the mmf F_m, we use (16)-(23). Equations (20)-(23) are derived from the collection of a high number of 3-D finite element computations.

$$R_m = \frac{h_m}{m_0 m_{rm} w_m l_f} \tag{16}$$

$$F_m = \frac{h_m B_r}{m_0 m_{rm}} \tag{17}$$

$$R_{Ccore} = \frac{l_{sw} + 2h_{sw} + (2\sqrt{2}+1)l_f}{m_0 m_{rFe} w_{sc} l_f} \tag{18}$$

$$R_{SScore} = \frac{l_{sw} + \sqrt{2}h_{sw} - 2l_f}{m_0 m_{rFe} w_{sc} l_f} \tag{19}$$

$$R_{LEC} = \frac{h_m}{m_0 w_m}\left(0.66 - 0.073 h_m + 2.6\times10^{-3} h_m^2 + \frac{0.012 w_{rc2} + 0.037 w_m}{h_m}\right) \tag{20}$$

$$R_{ctc} = \frac{1}{m_0 l_f}\left[0.63 - 0.060\frac{w_{sc}}{w_{rc2}} + 0.060\frac{w_{sc}^2}{w_{rc2}^2} + 0.21\frac{h_m}{w_{rc2}} + 0.082\frac{h_m^2}{w_{rc2}^2}\right] \tag{21}$$

$$R_g = \frac{g}{m_0 l_f w_{rc2}}\left[1.3 - 0.64\frac{w_{sc}}{w_{rc2}} + 0.17\frac{w_{sc}^2}{w_{rc2}^2} + 0.028\frac{w_{rc2}}{g} - 6.4\times10^{-4}\frac{w_{rc2}^2}{g^2} - 2.3\frac{g}{l_f} + 3.8\frac{g^2}{l_f^2}\right] \tag{22}$$

$$R_{side} = \frac{g}{m_0 l_f w_{rc2}}\left[1.6 + 0.49\frac{d}{g} - 0.93\frac{d}{w_{rc2}} - 1.04\frac{w_{sc}}{w_{rc2}} + 0.16\frac{w_{sc}}{g}\right] \tag{23}$$

Calculation of F_{smax}

The torque of the TFPM machine can be predicted from (9), if the magnetomotive force F_s fed into the stator winding is known. Since we are interested by the maximum available torque, we need to find F_{smax}, the maximum value of F_s. F_{smax} is determined from the expression of the flux $\Phi_{ps}(t)$ created by the armature reaction in the core of a salient TFPM machine, fed with a sinusoidal current.

$$\Phi_{ps}(t) = \frac{F_s}{4}\left(\sin d\left[\left(\frac{1}{R_{up}}+\frac{3}{R_{ap}}\right)\cos wt+\left(\frac{1}{R_{up}}-\frac{1}{R_{ap}}\right)\cos 3wt\right]\right)+\ldots$$

$$\ldots\frac{F_s}{4}\left(\cos d\left[\left(\frac{1}{R_{up}}+\frac{3}{R_{ap}}\right)\sin wt+\left(\frac{1}{R_{up}}-\frac{1}{R_{ap}}\right)\sin 3wt\right]\right) \quad (24)$$

The total flux flowing in one stator core of the TFPM machine is the sum of the no-load flux per pole $\Phi_{pnl}(t)$ and the flux $\Phi_{ps}(t)$ created by the armature reaction:

$$\Phi_{ptot}(t) = \Phi_{ps}(t) + \Phi_{pnl}\cos(vt - p) \quad (25)$$

The value of F_{smax} is limited by the saturation flux density B_{Fesat} in the stator core. The saturation flux is defined as:

$$\Phi_{psat} = B_{Fesat} w_{sc} l_f \quad (26)$$

To obtain F_{smax}, we vary $w\,t$ by software, between *0* and *2p*, and set Φ_{ptot} to its saturation flux Φ_{psat} defined by (26). Using (24) and (25), we can determine a certain value of $w\,t$ for which F_s is maximum.

In all calculations, the following values are used:

- J = 5.0 A/mm^2
- k_{sfill} = 0.5
- B_r = 1.23 T
- μ_{rFe} = 1000
- μ_{rm} = 1.09
- B_{FEsat} = 1.9 T
- δ = 0 degree

It must be noted that the optimization process targeted equal efficiency values for the two machine types. The targeted efficiency was 92%. This was made possible with current densities of 4 A/mm^2 for the Conventional PMSM, and 5 A/mm^2 for the TFPM machine.

Nomenclature

A_{Cus} , cross-section of one conductor in the slots
b_s , stator slot width
B_1 , Fundamental component of the no-load flux density
B_{Fesat} , Saturation flux density of laminated iron
B_g , no-load flux density in the air gap
B_r , remanent flux density
d , overlap distance between stator core and flux concentrator
E , rms no-load voltage
f , electrical frequency in Hz
F_m , PM equivalent magnetomotive force (mmf)
F_s , peak value of the stator magnetomotive force
F_{smax} , maximum value of Fs obtained at saturation
g , air gap thickness
h_m , magnet thickness
h_s , stator slot height
h_{sw} , height of stator winding in TFPM
h_w , thickness of the stator slot wedge
I , rms nominal phase current
J , current density in the conductors
k_{mag} , RFPM ratio of magnet width over pole pitch
k_{sfill} , slot filling factor
k_{ws} , skewing factor
K_{TFPM_Cost} , TFPM cost advantage factor
l_s , length of the stator stack of laminations
l_f , length of flux concentrator in axial direction
l_{sw} , width of stator winding in TFPM
L_a , stator inductance for rotor in aligned position
L_u , stator inductance for rotor in unaligned position
m , number of phases
N_{slot} , number of conductors per slot
p , number of pole pairs
P_{mech} , mechanical power on the machine shaft
q , number of slot per pole per phase
r_g , air gap radius
R_m , PM recoil reluctance
R_g , air gap reluctance
R_{stat_teeth} , reluctance of the stator teeth
R_{stat_yoke} , reluctance of the stator yoke
R_{rot_back} reluctance of the rotor back iron
R_{side} , TFPM reluctance of leakage path between stator core and flux concentrator in unaligned position
R_{up} , TFPM reluctance per pole pair seen by the stator conductors in unaligned position
R_{ap} , TFPM reluctance per pole pair seen by the stator conductors in aligned position
R_{Ccore} , reluctance of TFPM stator core on winding side
R_{SScore} , reluctance of TFPM stator core on opposite side
R_{LEC} , reluctance of leakage path between two adjacent flux concentrators
R_{ctc} , TFPM reluctance of leakage path between stator core and adjacent flux concentrator in aligned position
T , average continuous torque
w_m , magnet width in TFPM machine
w_{sc} , TFPM stator core width
w_{rc2} , width of flux concentrators
Φ_g , RFPM no-load flux in the air gap
Φ_{pnl} , TFPM no-load flux per pole in the stator core
Φ_{ps} , flux component created by the stator current in the core of a salient TFPM machine
Φ_{psat} , saturation flux in one pole of stator core of TFPM machine
Φ_{ptot} , sum of no-load flux and stator-created flux in one pole of the stator core of TFPM machine
μ_{rm} , PM recoil relative permeability
μ_{rFe} , relative permeability of laminated steel
τ_p , pole pitch
θ , phase angle between E and I
ω , electrical angular frequency in rad/s
Ω , machine angular rotational speed in rad/s